ACS OMEGA

http://pubs.acs.org/journal/acsodf

Article

Photocatalytic Reduction of Aqueous Nitrate with Hybrid Ag/g-C_3N_4 under Ultraviolet and Visible Light

Shelton J. P. Varapragasam, Jessica M. Andriolo, Jack L. Skinner, and Erik M. Grumstrup*

Cite This: *ACS Omega* 2021, 6, 34850−34856

Read Online

ACCESS | Metrics & More | Article Recommendations | Supporting Information

ABSTRACT: The concentration of nitrate in natural surface waters by agricultural runoff remains a challenging problem in environmental chemistry. One promising denitrification strategy is to utilize photocatalysts, whose light-driven excited states are capable of reducing nitrate to nitrogen gas. We have synthesized and characterized pristine and silver-loaded graphitic carbon nitrides and assessed their activity for photocatalytic nitrate reduction at neutral pH. While nitrate reduction does occur on the pristine material, the silver cocatalyst greatly enhances product yields. Kinetic studies performed in batch photoreactors under both UV and visible excitation suggest that nitrate reduction to produce aqueous nitrite, ammonium, and nitrogen gas proceeds via a cooperative water reduction on the silver metal domains to produce adsorbed H atoms. By varying the percentage of silver loading onto the g-C_3N_4, the density of metal domains can be adjusted, which in turn tunes the reduction selectivity toward various products.

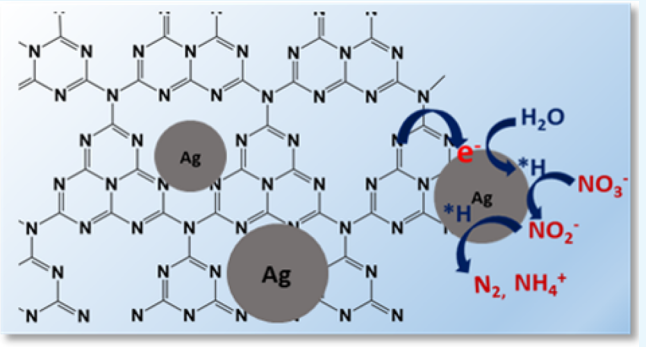

INTRODUCTION

The nitrogen cycle, which interconverts nitrogen between oxidized and reduced forms, is of central importance to agriculture, energy, and the environment. A significant recent driver of this cycle has been anthropogenic nitrogen fixation, primarily directed toward the nitrification of soils for agriculture but also toward applications in chemical synthesis and energy storage.[1−4] While essential for modern agriculture, anthropogenic nitrogen fixation is a significant perturbation to the nitrogen cycle, resulting in environmental degradation in the form of eutrophication of surface waters and contamination of groundwaters.[5−7] To rebalance the nitrogen cycle, identification of an artificial denitrification strategy that is distributable and can be implemented on a large scale is imperative.

In nature, denitrification primarily occurs via the sequential reduction of NO_x to N_2 in microbial organisms.[8−10] Contemporary water treatment approaches replicate this natural denitrification process, utilizing bacteria to catalyze the multi-step electron transfer pathway to convert NO_x into N_2. Although highly effective, this approach relies on large facilities that are resource intensive and centralized.[7] One alternative approach is to drive nitrate reduction on semiconductor photocatalysts activated by sunlight. Such photocatalytic nitrate reduction (PNR) schemes are promising alternatives for large-scale artificial denitrification as they could be incorporated into technologies that are highly distributable. Nevertheless, successful application of PNR is contingent on finding materials that are suitable in terms of efficiency, cost, selectivity toward N_2 formation, and environmental compatibility.

Although the transformation of nitrate into chemically stable reduced species occurs through a number of interrelated multistep reactions, the initial reduction of nitrate to its radical dianion ($E^0(NO_3^-/NO_3^{2-})$ = − 0.89 *V* vs SHE)[11,12] is electrochemically most demanding. This initial step follows one of two pathways. The vast majority of work in PNR exploits an indirect route in which an aqueous anion (often $CO_2^{\bullet-}$) is produced when an introduced hole scavenger (e.g., formic acid) is oxidized by the photoexcited semiconductor.[7] In a subsequent step, nitrate is reduced by the intermediate aqueous radical anion, which has a reduction potential more negative than that of the $NO_3^-/NO_3^{\bullet 2-}$ couple. Thus, the oxidation potential of the photogenerated holes, together with the ensuing radical chemistry of the hole scavenger, determines the initial yield of the first stable intermediate, NO_2^-. To date, most efforts in PNR have focused on TiO_2 as a light absorber and catalyst.[13−15] Because TiO_2 has a conduction band (CB) edge (−0.13 V vs SHE at pH = 0) that is more positive than the one electron reduction of nitrate,[16,17] it is generally

Received: October 4, 2021
Accepted: November 26, 2021
Published: December 10, 2021

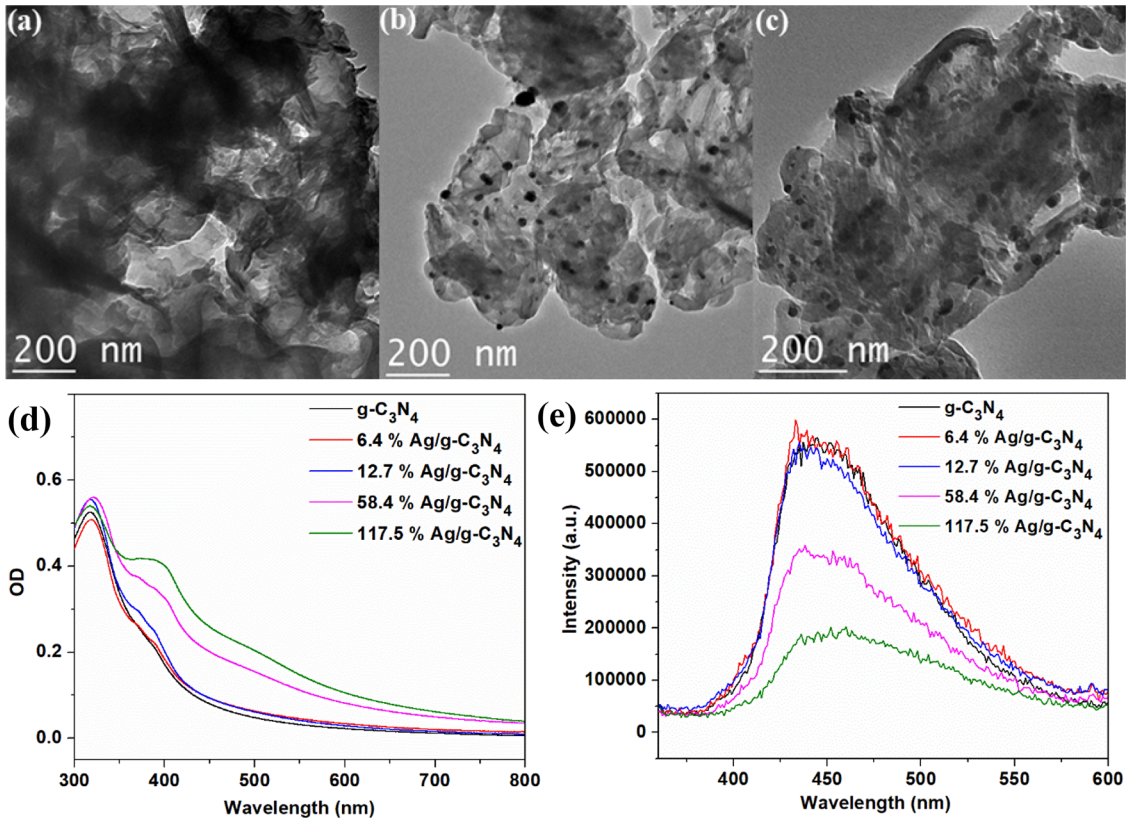

Figure 1. TEM images of (a) g-C_3N_4, (b) 6.4% Ag/g-C_3N_4, and (c) 12.7% Ag/g-C_3N_4. (d) UV−vis absorption spectra and (e) emission spectra of pristine g-C_3N_4 and hybrid Ag/g-C_3N_4 materials.

accepted that PNR with TiO_2 proceeds via the indirect mechanism described above. On the other hand, if the reduction potential of the CB is sufficiently negative, then the photogenerated electrons can directly reduce nitrate to the radical dianion. This second, direct path to PNR utilizes photogenerated electrons (and not holes) to initialize the reduction reaction.[18]

Regardless of the initial reduction path, the transformation of NO_3^- to NO_2^-, the first stable intermediate, is a two-proton, two-electron process. As described in detail in the review of Tugaoen et al., further reduction of nitrite proceeds through a complex series of coupled reactions that, regardless of whether ammonium or nitrogen gas is the product, requires another six electrons and eight protons.[7] Most published work to date has fulfilled the requirement for protons by using formic acid as a hole scavenger, which lowers the pH of the reaction vessel to ∼2.5.[13,14,19−22] However, in most natural water systems, the pH is near neutral. It is therefore essential to find potential PNR photocatalysts that provide not only a high current of electrons (of sufficient reduction potential) but also a steady stream of protons or adsorbed H atoms at circumneutral pH.[23−25]

This work describes initial efforts at utilizing graphitic carbon nitride (g-C_3N_4) to meet the stringent demands of nitrate reduction. g-C_3N_4 possesses a conduction band energy (−1.3 V vs SHE)[26−28] sufficient for the direct one-electron reduction of nitrate and therefore is a promising candidate for initializing direct nitrate reduction in the absence of a hole scavenger. Additionally, g-C_3N_4 is inexpensive, stable under photocatalytic conditions, and environmentally benign.[29] Both pure g-C_3N_4 and Ag/g-C_3N_4 hybrid photocatalysts were studied, with the hybrid system exhibiting faster reduction rates under both visible and UV photoexcitation. The rate of nitrate reduction under UV light illumination is faster than that under visible light irradiation. Reduction of NO_3^- to NO_2^- is independent of silver metal loading onto g-C_3N_4; however, varying the silver loading appears to modify product selectivity toward nitrogen gas or ammonium. Excitation wavelength-dependent kinetic studies suggest that reduction of nitrate likely proceeds first via photocatalytic water reduction to form chemisorbed hydrogen (*H) on the Ag surface, which in turn reduces nitrate to its radical dianion.

RESULTS AND DISCUSSION

Materials Characterization. Figure 1 highlights transmission electron microscopy (TEM) and spectroscopic characterization of the pristine and hybrid materials. Panel a shows the TEM image of as-prepared pure g-C_3N_4. The higher contrast dark dots in panels b and c are regions of deposited silver metal. As the weight percentage of the silver nanoparticle increases from 6.4 to 117.5%, the number of decorated silver nanoparticles on the g-C_3N_4 increases (SI). While it is difficult to confidently determine an accurate distribution of nanoparticle sizes from a limited number of TEM images, particle size histograms (Figure S3) show that the particle sizes generally range from 10 to 100 nm in diameter, with larger diameters more prevalent at higher mass loadings.

Panel d of Figure 1 shows the absorption spectrum of pristine g-C_3N_4, which is consistent with a previously reported bandgap energy of 2.7 eV.[26] For the hybrid materials, an additional broader absorption band can be observed between ∼450 and ∼ 550 nm, attributable to the surface plasmon

https://doi.org/10.1021/acsomega.1c05523
ACS Omega 2021, 6, 34850−34856

resonance of the silver nanoparticles. The absorbance of this redshifted peak increases as silver loading is increased from 6.4 to 117.5%, confirming a larger population of silver metal nanoparticles with greater mass loadings.

The effects of increased silver loading on photoluminescence (PL) yield can be seen in Figure 1e, which shows emission spectra of g-C_3N_4 and Ag/g-C_3N_4 collected after excitation at 310 nm for identical OD samples. Pure g-C_3N_4 shows the highest relative emission intensity, with evidence of quenching as silver loading is increased in the hybrid Ag/g-C_3N_4 materials. The emission quenching observed in the hybrid Ag/g-C_3N_4 is likely due to charge transfer from the g-C_3N_4 semiconductor to the silver metal nanoparticle, preventing radiative recombination of the photogenerated excited state.[33−35] Note, however, that extensive quenching of the PL is not observed until the highest two Ag loadings, suggesting that many emissive states have insufficient mobility to encounter an Ag particle during their lifetime.[36,37]

Photocatalytic Nitrate Reduction under UV Light. To evaluate the photocatalytic nitrate reduction activity of g-C_3N_4, batch reactor studies were performed with 360 nm illumination over 8 h using methanol as a hole scavenger.[26,38−40] Figure 2 summarizes the fractional NO_2^-, N_2, and NH_4^+ composition of the reaction mixture after 8 h of illumination under UV illumination for pristine g-C_3N_4 and Ag/g-C_3N_4 catalysts with increasing Ag loading. The reported values represent averages of two or three separate runs (Table S1).

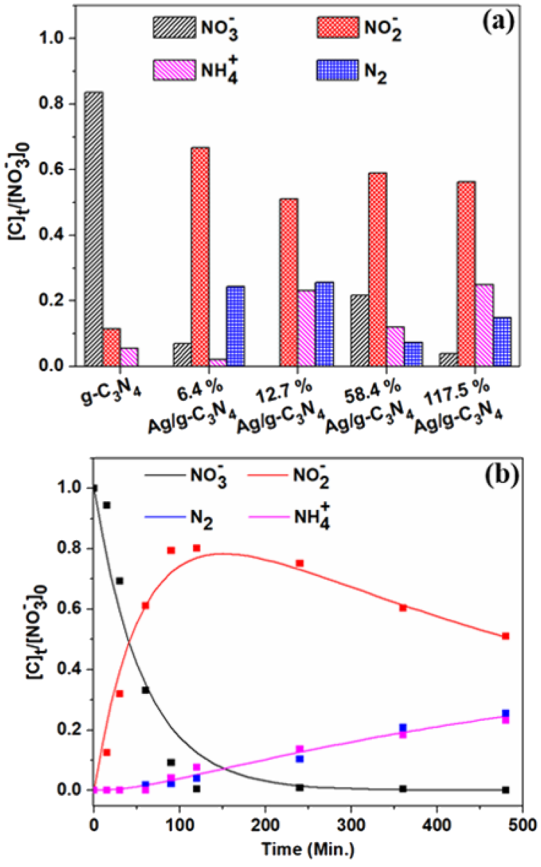

Figure 2. (a) Comparison of photocatalytic NO_3^- reduction into different reduced nitrogen species over pristine and silver-loaded g-C_3N_4 under UV light. (b) Fractional nitrogen kinetics (with respect to initial nitrate concentration) for 12.7% Ag/g-C_3N_4 under 360 nm irradiation for 8 h. The solid lines show the global best fit to the data using the kinetic model of scheme 1. Note that N_2 and NH_4^+ fits are superimposed.

The results from the batch reactor studies show that pristine g-C_3N_4 is photocatalytically active, reducing 16.5% of the nitrate over the course of an 8 h reaction time. The majority of the (non-NO_3^-) nitrogen remains as nitrite (11.5%) with 5% converted to aqueous ammonium. While promising, we speculated that the incomplete reduction of nitrate on pristine g-C_3N_4 was due to rapid electron−hole recombination, as is well known to occur in g-C_3N_4.[41,42] In an effort to improve the PNR efficiency, we used silver as a cocatalyst to facilitate electron−hole separation. Comparison of the PNR batch reactor studies for the various silver-loaded hybrid Ag/g-C_3N_4 materials shows that the presence of Ag dramatically improves the reduction of nitrate. Indeed, under the same conditions, Ag/g-C_3N_4 shows almost complete reduction of nitrate, regardless of the loading. This result is somewhat surprising, given that significant PL quenching occurs only at loadings greater than 12.7% (Figure 1e). However, we note that the PL quantum yield of g-C_3N_4 is low (∼5%),[43] suggesting that PL may be relatively insensitive to the charge separation process expected to occur at the Ag−g-C_3N_4 interface. Transient absorption spectroscopies are likely to provide further insight into excited state branching ratios as these techniques are sensitive to both emissive and non-emissive states. Regardless of the Ag loading level, the majority product was nitrite, with little trend observable as the loading increased from 6.4 to 117.5%. However, it appears that increased loading tends to favor ammonium production, with the lowest loadings of 6.4 and 12.7% favoring N_2 relative to NH_4^+. Control studies performed using the 12.7% Ag/g-C_3N_4 photocatalyst in the absence of irradiation or in the absence of methanol showed no change in nitrate concentration over an 8 h reaction time, confirming that both light irradiation and the presence of methanol are necessary for PNR.

To further elucidate the reduction process, we measured reaction kinetics by withdrawing aliquots from the 12.7% Ag/g-C_3N_4 reaction mixture during UV illumination. Figure 2b summarizes the results from these studies in terms of fractional N concentration. Within the first 2 h, the nitrate concentration drops to below the detection limit concomitant with a rise in nitrite concentration. These relatively rapid kinetics are followed by a slow decrease in nitrite concentration, while ammonia and nitrogen gas concentrations rise. Inspection of the experimental data suggests that the PNR process can be approached with a relatively simple model, namely a pseudo-first-order process in which nitrate is rapidly converted to nitrite, followed by a slower reduction of nitrite to nitrogen gas and ammonium with a similar rate, as described by Scheme 1.

Scheme 1. Pseudo-first Order Nitrate Reduction Model

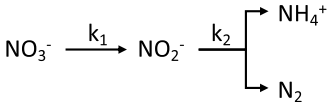

While the model outlined by Scheme 1 is clearly too simple to capture all the mechanistic complexity of the multi-proton, multi-electron reduction process, our experimental data are well described by a global fit of the model, as can be seen in Figure 2b (solid lines) with effective rate constants $k_1 = 1.7 \pm 0.1 \times 10^{-2}$ min^{-1} and $k_2 = 8.1 \pm 0.8 \times 10^{-4}$ min^{-1}.

https://doi.org/10.1021/acsomega.1c05523
ACS Omega 2021, 6, 34850−34856

Photocatalytic Nitrate Reduction under Visible Light. To further elucidate the PNR process on pristine g-C_3N_4 and hybrid Ag/g-C_3N_4 materials, we performed analogous photocatalytic studies with 425 nm illumination on the pristine g-C_3N_4 and 12.7% Ag/g-C_3N_4 samples, as summarized in Figure 3. For the pristine g-C_3N_4, no reduction of nitrate was

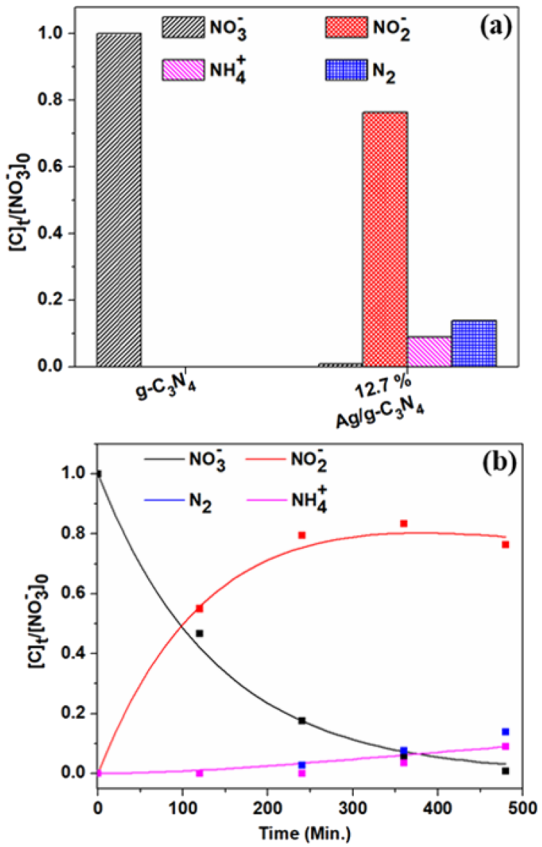

Figure 3. (a) Comparison of PNR under 425 nm illumination for pristine g-C_3N_4 and 12.7% Ag/g-C_3N_4 on NO_3^-. (b) Kinetics of nitrogen species with respect to initial nitrate amount during the photocatalytic nitrate reduction over 12.7% Ag/g-C_3N_4 under visible light for 8 h.

observed under 425 nm illumination. In contrast, for the hybrid Ag/g-C_3N_4 photocatalyst, nitrate is completely reduced over the course of the reaction. Kinetics shown in Figure 3b indicate that both nitrate removal and formation of products occur more slowly than those collected under 360 nm excitation (Figure 2b). For the 425 nm photocatalytic studies, a global fit of the data to the first-order model described above recovers effective rate constants of $k_1 = 7.2 \pm 0.3 \times 10^{-3}$ min^{-1} and $k_2 = 2.9 \pm 0.3 \times 10^{-4}$ min^{-1}. These fit-extracted rate constants at 425 nm represent a slowdown of the reaction by 2.4 ± 0.2 for k_1 and 2.8 ± 0.4 for k_2 relative to photoexcitation at 360 nm. Importantly, this difference is not because of lower excitation densities. In fact, while the absorptance of both the pristine and hybrid materials at 425 nm is lower than that at 360 nm by a factor of ~2.3, the photon flux of the 425 nm reactor is more than 17 times higher than that of the UV 360 nm reactor. Therefore, if excitation at the two wavelengths were equivalent, then we would expect that k_1 would be ~7 times larger (17/2.3) at 425 nm than at 360 nm. Thus, the observed difference in rates suggests that excitation at 425 nm creates g-C_3N_4 excited states that are approximately 17-fold less effective at driving nitrate reduction.

To understand these results, we next turned to evaluating the activity of the 12.7% Ag/g-C_3N_4 material for photocatalytic water reduction (PWR) in the absence of aqueous nitrate. These measurements were motivated by previous work reporting nitrate reduction via hydrogenation in the presence of noble metal (Pt or Pd) surfaces (without photoexcitation but with H_2 gas present).[44−51] After an 8 h reaction period, hydrogen gas evolved from the 12.7% Ag/g-C_3N_4 reaction mixture was quantified by GC. For the 360 nm reactor, 20 μmol of H_2 was generated, yielding a calculated hydrogen evolution rate of 210 μmol/g·cat/h. For 425 nm excitation, 3.7 μmol of H_2 was generated, with a calculated rate of 39 μmol/g·cat/h. Just as in the PNR studies performed above, we observe a slowdown of PWR when the excitation wavelength is shifted from the UV into the visible range. However, in the case of PWR, there is a 5.4-fold slowdown of the H_2 evolution rate compared to the 2.4-fold slowdown in the nitrate removal kinetics (k_1).

This discrepancy in rates is consistent with the nitrate hydrogenation study of Pintar and co-workers,[48] who varied H_2 partial pressures on a Pd/Cu bimetal catalyst to determine that the nitrate loss rate has a reaction order in H_2 of $n = 1/2$, attributable to the key role played by the metal-adsorbed hydrogen atom, *H, as a reactant in the loss of nitrate. If for photocatalytic nitrate reduction, generation of hydrogen via PWR is the rate-limiting step in nitrate reduction (to nitrite), then the ratio of PNR rate constants at UV and visible excitation conditions should be equal to the square root of the H_2 generation rates for PWR, that is $k_1^{UV}/k_1^{vis} = (k_{PWR}^{UV}/k_{PWR}^{vis})^{1/2}$. Within error, the rates we determine are consistent with this interpretation.

The above results showing spectral variation in reaction rate, together with the previously reported $p_{H_2}^{1/2}$ dependence of nitrate loss, allow us to propose the following mechanism for nitrate reduction (to nitrite) in the hybrid Ag/g-C_3N_4 system. Note that this mechanism is largely consistent with that compiled in a review by Tugaoen et al.,[7] with the exception that this system appears to proceed via an initial reduction step involving an adsorbed hydrogen atom *H produced via photocatalytic water reduction. Nitrate adsorbed on a nearby site can react with *H, forming NO_3^{2-} (reaction 1), which is quickly hydrolyzed to form $NO_2^{\cdot}$ (reaction 2). This radical species is readily reduced by the hybrid catalyst, given that even a conservative estimate of the flat band potential of the n-type hybrid catalyst system, $(E_{VB} + E_{CB})/2-0$ V vs SHE[52,53] is well negative of the $NO_2^{\cdot}/NO_2^-$ couple ($E_0 = +1.04$ V vs SHE) (reaction 3).

$$NO_3^- + {}^*H \rightarrow NO_3^{2-} + H^+ \quad (1)$$

$$NO_3^{2-} + H_2O \rightarrow NO_2^{\cdot} + 2OH^- \quad (2)$$

$$NO_2^{\cdot} + e^- \rightarrow NO_2^- \quad (3)$$

Regardless of the excitation wavelength (360 or 425 nm), the subsequent reduction of nitrite (k_2 in Scheme 1) proceeds with an effective rate constant that is between 20 and 25 times slower than nitrate reduction (k_1 in Scheme 1). However, the ratio of the nitrite reduction rate constants is identical (within error) to the ratio of k_1 rate constants, $k_1^{UV}/k_1^{vis} = 2.4 \pm 0.2 \approx k_2^{UV}/k_2^{Vis} = 2.8 \pm 0.4$. Although this parity might be coincidental, it is interesting to note that a plausible

https://doi.org/10.1021/acsomega.1c05523
ACS Omega 2021, 6, 34850−34856

mechanism for the reduction of nitrite can be expressed via a nearly identical set of steps as nitrate reduction, outlined in reactions 4–6.

$$NO_2^- + {}^*H \rightarrow NO_2^{\cdot 2-} + H^+ \quad (4)$$

$$NO_2^{\cdot 2-} + H_2O \rightarrow NO^{\cdot} + 2OH^- \quad (5)$$

$$NO^{\cdot} + e^- \rightarrow NO^- \quad (6)$$

The similarities in the sets of reactions (1–3 vs 4–6) are striking. For reaction 4, $E^0(NO_2^-/NO_2^{\cdot 2-}) = -0.47$ V vs SHE.[54] In principle, the photogenerated electrons in the hybrid catalyst system should have a sufficiently negative potential to reduce nitrate, however, reaction 4, in which the initial reduction of nitrite is instead mediated by adsorbed hydrogen, would be consistent with previous nitrite hydrogenation studies that suggest that the adsorbed hydrogen atom is a reactant in the nitrite loss reaction.[45,55] The second hydrolysis step (reaction 5) occurs rapidly, and the final electron transfer (reaction 6) can readily occur in the presence of the Ag/C_3N_4 system since $E^0(NO^{\cdot}/NO^-) = +0.47$ V,[54] well positive of the flat band potential of the hybrid catalyst.

The pathways by which nitrite is reduced to form N_2 and NH_4^+ have been extensively studied, although characterization of the intermediates that lead to the formation of the final stable species has proved challenging.[45,46,56] While the results we show here are insufficient to ascribe a mechanism for the formation of N_2 and NH_4^+, it is worth highlighting that in hydrogenation studies, nitrite reduction generally proceeds much more quickly than the initial reduction of nitrate to nitrite.[55] Here, the opposite effect is observed, perhaps highlighting that for these photocatalytic systems, back reactions that regenerate nitrite (from the many single electron reduction intermediates en route to N_2 or NH_4^+) may be important.

$$NO_2^- + 6e^- + 8H^+ \rightarrow NH_4^+ + 2H_2O \quad (7)$$

$$2NO_2^- + 6e^- + 8H^+ \rightarrow N_2 + 4H_2O \quad (8)$$

Regardless of the mechanism, some insight can be gained by comparing the selectivity toward nitrogen gas as a function of silver loading (Figure 2a). Although the primary product in all cases is NO_2^-, it appears that lower Ag loading favors formation of N_2 over NH_4^+. This trend likely reflects differences in the H_2 formation rates for various loadings. The TEM images in Figure 1 show that at higher Ag loading, the size and density of silver metal domains on the g-C_3N_4 semiconductor increases. The increased Ag loading will lead to greater H_2 production rates due to higher efficiency separating photogenerated electrons and holes (see Figure 1e). Previous nitrate hydrogenation studies have shown that selectivity toward N_2 is greater at low H_2 concentrations and selectivity toward ammonium increases when the H_2 concentration increases.[57,58]

In summary, photocatalysts of pristine g-C_3N_4 and hybrid Ag/g-C_3N_4 of different silver metal loadings were successfully prepared via a facile photochemical deposition method. While pristine g-C_3N_4 does photocatalytically reduce NO_3^- at circumneutral pH, the hybrid Ag/g-C_3N_4 shows significantly enhanced PNR under both UV- and visible light-irradiated conditions, perhaps due to an enhancement of electron–hole separation in the hybrid material. Time-resolved spectroscopic studies, which investigate the dynamics of charge separation in the Ag-loaded C_3N_4, will be the subject of a forthcoming work. By varying the percentage of the metal loading, we are able to adjust the number density of cocatalyst Ag metal nanoparticles on the g-C_3N_4 semiconductor, which tunes the selectivity of reduction products. Although the current hybrid material efficiently reduces NO_3^-, a future work will focus on enhancing both the rate and selectivity of NO_2^- reduction through C_3N_4 defect passivation as well as bimetal cocatalyst loading.

MATERIALS AND METHODS

Synthesis and Materials Characterization. We have adopted previously reported protocols for the synthesis of pristine g-C_3N_4 and the hybrid silver-loaded Ag/g-C_3N_4 (SI).[30−32] Prepared pristine and hybrid materials were characterized with transmission electron microscopy, X-ray diffraction, and several spectroscopic techniques to confirm the deposition of silver nanoparticles on the g-C_3N_4 material, as detailed below and in the Supporting Information.

Photocatalytic Studies. PNR studies were performed in a 100 mL round-bottom quartz flask in a neutral aqueous solution. Twelve milligrams of photocatalyst, 10 mL of 400 μM $NaNO_3$ stock solution, 2 mL of methanol, and a magnetic stirrer were added to the quartz flask. After the mixture was sonicated for 3 min, the flask was sealed with a rubber septum and purged with Ar gas for an hour and placed in a photoreactor. For UV irradiation studies, the reaction was carried out in a Rayonet RPR 100 photochemical reactor (Southern New England Ultraviolet Co.) The photoreactor is equipped with low-pressure Hg lamps that are coated with phosphor and spectrally filtered to pass 360 nm with an average irradiance of 2.3 mW/cm^2. For visible-light studies, reactions were carried out in a photocatalytic reactor (HepatoChem, HCK1006-01-023) with a 425 nm (20 nm FWHM) LED light source with a 33 mW/cm^2 average irradiance. Photoreactor spectra can be found in the Supporting Information.

PWR studies were conducted by placing 12 mg of photocatalyst, 10 mL of Millipore water (18.2 MΩ), 2 mL of methanol, and a magnetic stirrer in a 100 mL flask. The flask was sealed and sonicated for 3 min, purged with Ar gas for an hour, and irradiated with either a 360 or 425 nm light source as above. For quantifying gas species, a 250 μL gas sample was withdrawn from the headspace of the reactor at regular intervals for GC analysis.

Analytical methods. Concentrations of NO_3^- and NO_2^- were determined using a flow injector analysis LACHAT instrument (QuikChem 8500), and the NH_4^+ concentration was determined via a Timberline Instruments TL-2800 Ammonia Analyzer (details in the SI). GC was used to qualitatively confirm formation of N_2; however, quantification of N_2 was prevented by variable N_2 leakage into the flask during photoreaction runs. As a result, reported N_2 amounts are calculated by mass (N) balance. The nitrate reduction and the reduced nitrogen species selectivity were calculated as follows

$$\%\ \text{of}[NO_3^-]\text{reduction} = \frac{[NO_3^-]_t}{[NO_3^-]_0} \quad (9)$$

$$\%\ \text{of}[NO_2^-/NH_4^+]\text{selectivity} = \frac{[NO_2^-/NH_4^+]_t}{[NO_3^-]_0} \quad (10)$$

https://doi.org/10.1021/acsomega.1c05523
ACS Omega 2021, 6, 34850−34856

where subscripts 0 and t represent the concentration of the species at the initial and t h/min of the reaction interval, respectively.

■ ASSOCIATED CONTENT

Supporting Information

The Supporting Information is available free of charge at https://pubs.acs.org/doi/10.1021/acsomega.1c05523.

Preparation of g-C_3N_4 and Ag/g-C_3N_4; TEM images of 58.4 and 117.5% Ag-loaded g-C_3N_4; size distribution of Ag nanoparticles of 6.4% Ag/g-C_3N_4, 12.7% Ag/g-C_3N_4, and 58.4% Ag/g-C_3N_4; XRD patterns and XPS spectra of all materials; Emission spectra of light sources of both UV and visible photocatalytic reactors; and raw data tables associated with Figures 2 and 3 (PDF)

■ AUTHOR INFORMATION

Corresponding Author

Erik M. Grumstrup − *Department of Chemistry and Biochemistry, Montana State University, Bozeman, Montana 59717, United States;* orcid.org/0000-0002-0568-3889; Email: erik.grumstrup@montana.edu

Authors

Shelton J. P. Varapragasam − *Department of Chemistry and Biochemistry, Montana State University, Bozeman, Montana 59717, United States*

Jessica M. Andriolo − *Department of Mechanical Engineering, Montana Technological University, Butte, Montana 59701, United States*

Jack L. Skinner − *Department of Mechanical Engineering, Montana Technological University, Butte, Montana 59701, United States*

Complete contact information is available at: https://pubs.acs.org/10.1021/acsomega.1c05523

Funding

This material is based upon work supported in part by the National Science Foundation EPSCoR Cooperative Agreement OIA-1757351.

Notes

The authors declare no competing financial interest.

■ REFERENCES

(1) Valera-Medina, A.; Xiao, H.; Owen-Jones, M.; David, W. I. F.; Bowen, P. J. Ammonia for power. *Prog. Energy Combust. Sci.* **2018**, *69*, 63−102.

(2) Valera-Medina, A.; Amer-Hatem, F.; Azad, A. K.; Dedoussi, I. C.; de Joannon, M.; Fernandes, R. X.; Glarborg, P.; Hashemi, H.; He, X.; Mashruk, S.; McGowan, J.; Mounaim-Rouselle, C.; Ortiz-Prado, A.; Ortiz-Valera, A.; Rossetti, I.; Shu, B.; Yehia, M.; Xiao, H.; Costa, M. Review on Ammonia as a Potential Fuel: From Synthesis to Economics. *Energy Fuels* **2021**, 6964.

(3) Chen, J. G.; Crooks, R. M.; Seefeldt, L. C.; Bren, K. L.; Bullock, R. M.; Darensbourg, M. Y.; Holland, P. L.; Hoffman, B.; Janik, M. J.; Jones, A. K.; Kanatzidis, M. G.; King, P.; Lancaster, K. M.; Lymar, S. V.; Pfromm, P.; Schneider, W. F.; Schrock, R. R. Beyond fossil fuel−driven nitrogen transformations. *Science* **2018**, *360*, No. eaar6611.

(4) Atkins, P. W. T. L. O.; Rourke, J. P.; Weller, M. T.; Armstrong, a. F. A. *Shriver and Atkins' Inorganic Chemistry*; OUP Oxford, 2010, 379−390.

(5) Bernhard, A. The Nitrogen Cycle: Processes, Players, and Human Impact. *Nat. Educ. Know.* **2010**, 25.

(6) Stein, L. Y.; Klotz, M. G. The nitrogen cycle. *Curr. Biol.* **2016**, *26*, R94−R98.

(7) Tugaoen, H. O. N.; Garcia-Segura, S.; Hristovski, K.; Westerhoff, P. Challenges in photocatalytic reduction of nitrate as a water treatment technology. *Sci. Total Environ.* **2017**, *599-600*, 1524−1551.

(8) Skiba, U. Denitrification. In *Encyclopedia of Ecology*; Jørgensen, S. E.; Fath, B. D., Eds. Academic Press: Oxford, 2008; pp. 866−871.

(9) Martens, D. A. DENITRIFICATION. In *Encyclopedia of Soils in the Environment*; Hillel, D., Ed. Elsevier: Oxford, 2005; pp. 378−382.

(10) Maia, L. B.; Moura, J. J. G. How Biology Handles Nitrite. *Chem. Rev.* **2014**, *114*, 5273−5357.

(11) Cook, A. R.; Dimitrijevic, N.; Dreyfus, B. W.; Meisel, D.; Curtiss, L. A.; Camaioni, D. M. Reducing Radicals in Nitrate Solutions. The NO32- System Revisited. *Am. J. Phys. Chem. A* **2001**, *105*, 3658−3666.

(12) Fessenden, R. W.; Meisel, D.; Camaioni, D. M. Addition of Oxide Radical Ions (O^-) to Nitrite and Oxide Ions (O^{2-}) to Nitrogen Dioxide. *J. Am. Chem. Soc.* **2000**, *122*, 3773−3774.

(13) Ren, H.-T.; Jia, S.-Y.; Zou, J.-J.; Wu, S.-H.; Han, X. A facile preparation of Ag_2O/P25 photocatalyst for selective reduction of nitrate. *Appl. Catal., B* **2015**, *176-177*, 53−61.

(14) Luiz, D. d. B.; Andersen, S. L. F.; Berger, C.; José, H. J.; Moreira, R. d. F. P. M. Photocatalytic reduction of nitrate ions in water over metal-modified TiO_2. *J. Photochem. Photobiol., A* **2012**, *246*, 36−44.

(15) Sá, J.; Agüera, C. A.; Gross, S.; Anderson, J. A. Photocatalytic nitrate reduction over metal modified TiO_2. *Appl. Catal., B* **2009**, *85*, 192−200.

(16) Linsebigler, A. L.; Lu, G.; Yates, J. T. Photocatalysis on TiO_2 Surfaces: Principles, Mechanisms, and Selected Results. *Chem. Rev.* **1995**, *95*, 735−758.

(17) Roy, S. Photocatalytic Materials for Reduction of Nitroarenes and Nitrates. *J. Phys. Chem. C* **2020**, *124*, 28345−28358.

(18) Liu, G.; You, S.; Ma, M.; Huang, H.; Ren, N. Removal of Nitrate by Photocatalytic Denitrification Using Nonlinear Optical Material. *Environ. Sci. Technol.* **2016**, *50*, 11218−11225.

(19) Tugaoen, H. O. N.; Herckes, P.; Hristovski, K.; Westerhoff, P. Influence of ultraviolet wavelengths on kinetics and selectivity for N-gases during TiO_2 photocatalytic reduction of nitrate. *Appl. Catal., B* **2018**, *220*, 597−606.

(20) Doudrick, K.; Monzón, O.; Mangonon, A.; Hristovski, K.; Westerhoff, P. Nitrate Reduction in Water Using Commercial Titanium Dioxide Photocatalysts (P25, P90, and Hombikat UV100). *J. Environ. Eng.* **2012**, *138*, 852−861.

(21) Bems, B.; Jentoft, F. C.; Schlögl, R. Photoinduced decomposition of nitrate in drinking water in the presence of titania and humic acids. *Appl. Catal., B* **1999**, *20*, 155−163.

(22) Lucchetti, R.; Onotri, L.; Clarizia, L.; Natale, F. D.; Somma, I. D.; Andreozzi, R.; Marotta, R. Removal of nitrate and simultaneous hydrogen generation through photocatalytic reforming of glycerol over "in situ" prepared zero-valent nano copper/P25. *Appl. Catal., B* **2017**, *202*, 539−549.

(23) Hirayama, J.; Kondo, H.; Miura, Y.-k.; Abe, R.; Kamiya, Y. Highly effective photocatalytic system comprising semiconductor photocatalyst and supported bimetallic non-photocatalyst for selective reduction of nitrate to nitrogen in water. *Catal. Commun.* **2012**, *20*, 99−102.

(24) Ranjit, K. T.; Varadarajan, T. K.; Viswanathan, B. Photocatalytic reduction of nitrite and nitrate ions to ammonia on Ru/TiO_2 catalysts. *J. Photochem. Photobiol., A* **1995**, *89*, 67−68.

(25) Akihiko, K.; Kazunari, D.; Ken-ichi, M.; Takaharu, O. Photocatalytic Reduction of NO_3^- to Form NH_3 over Pt−TiO_2. *Chem. Lett.* **1987**, *16*, 1019−1022.

(26) Wang, X.; Maeda, K.; Thomas, A.; Takanabe, K.; Xin, G.; Carlsson, J. M.; Domen, K.; Antonietti, M. A metal-free polymeric photocatalyst for hydrogen production from water under visible light. *Nat. Mater.* **2009**, *8*, 76−80.

(27) Zheng, Y.; Lin, L.; Wang, B.; Wang, X. Graphitic Carbon Nitride Polymers toward Sustainable Photoredox Catalysis. *Angew. Chem., Int. Ed.* **2015**, *54*, 12868−12884.
(28) Wang, X.; Blechert, S.; Antonietti, M. Polymeric Graphitic Carbon Nitride for Heterogeneous Photocatalysis. *ACS Catal.* **2012**, *2*, 1596−1606.
(29) Xiong, W.; Huang, F.; Zhang, R.-Q. Recent developments in carbon nitride based films for photoelectrochemical water splitting. *Sustainable Energy Fuels* **2020**, *4*, 485−503.
(30) Qin, J.; Huo, J.; Zhang, P.; Zeng, J.; Wang, T.; Zeng, H. Improving the photocatalytic hydrogen production of Ag/g-C_3N_4 nanocomposites by dye-sensitization under visible light irradiation. *Nanoscale* **2016**, *8*, 2249−2259.
(31) Chan, S. C.; Barteau, M. A. Preparation of Highly Uniform Ag/TiO_2 and Au/TiO_2 Supported Nanoparticle Catalysts by Photodeposition. *Langmuir* **2005**, *21*, 5588−5595.
(32) Faisal, M.; Ismail, A. A.; Harraz, F. A.; Al-Sayari, S. A.; El-Toni, A. M.; Al-Assiri, M. S. Synthesis of highly dispersed silver doped g-C_3N_4 nanocomposites with enhanced visible-light photocatalytic activity. *Mater. Des.* **2016**, *98*, 223−230.
(33) Wang, J.; Cong, J.; Xu, H.; Wang, J.; Liu, H.; Liang, M.; Gao, J.; Ni, Q.; Yao, J. Facile Gel-Based Morphological Control of Ag/g-C_3N_4 Porous Nanofibers for Photocatalytic Hydrogen Generation. *ACS Sustainable Chem. Eng.* **2017**, *5*, 10633−10639.
(34) Li, Z.; Wang, J.; Zhu, K.; Ma, F.; Meng, A. Ag/g-C_3N_4 composite nanosheets: Synthesis and enhanced visible photocatalytic activities. *Mater. Lett.* **2015**, *145*, 167−170.
(35) Liu, R.; Yang, W.; He, G.; Zheng, W.; Li, M.; Tao, W.; Tian, M. Ag-Modified g-C_3N_4 Prepared by a One-Step Calcination Method for Enhanced Catalytic Efficiency and Stability. *ACS Omega* **2020**, *5*, 19615−19624.
(36) Merschjann, C.; Tyborski, T.; Orthmann, S.; Yang, F.; Schwarzburg, K.; Lublow, M.; Lux-Steiner, M. C.; Schedel-Niedrig, T. Photophysics of polymeric carbon nitride: An optical quasimonomer. *Phys. Rev. B* **2013**, *87*, 205204.
(37) Choudhury, B.; Paul, K. K.; Sanyal, D.; Hazarika, A.; Giri, P. K. Evolution of Nitrogen-Related Defects in Graphitic Carbon Nitride Nanosheets Probed by Positron Annihilation and Photoluminescence Spectroscopy. *J. Phys. Chem. C* **2018**, *122*, 9209−9219.
(38) Jiang, D.; Chen, L.; Xie, J.; Chen, M. Ag_2S/g-C_3N_4 composite photocatalysts for efficient Pt-free hydrogen production. The co-catalyst function of Ag/Ag2S formed by simultaneous photodeposition. *Dalton Trans.* **2014**, *43*, 4878−4885.
(39) Ge, L.; Han, C.; Liu, J.; Li, Y. Enhanced visible light photocatalytic activity of novel polymeric g-C_3N_4 loaded with Ag nanoparticles. *Appl. Catal., A* **2011**, *409-410*, 215−222.
(40) Roy, S. Tale of Two Layered Semiconductor Catalysts toward Artificial Photosynthesis. *ACS Appl. Mater. Interfaces* **2020**, *12*, 37811−37833.
(41) Maeda, K.; Wang, X.; Nishihara, Y.; Lu, D.; Antonietti, M.; Domen, K. Photocatalytic Activities of Graphitic Carbon Nitride Powder for Water Reduction and Oxidation under Visible Light. *J. Phys. Chem. C* **2009**, *113*, 4940−4947.
(42) Kumar, S.; Karthikeyan, S.; Lee, A. F. g-C_3N_4-Based Nanomaterials for Visible Light-Driven Photocatalysis. *Catalysts* **2018**, *8*, 74.
(43) Zhang, X.; Xie, X.; Wang, H.; Zhang, J.; Pan, B.; Xie, Y. Enhanced Photoresponsive Ultrathin Graphitic-Phase C_3N_4 Nanosheets for Bioimaging. *J. Am. Chem. Soc.* **2013**, *135*, 18−21.
(44) Yoshinaga, Y.; Akita, T.; Mikami, I.; Okuhara, T. Hydrogenation of Nitrate in Water to Nitrogen over Pd−Cu Supported on Active Carbon. *J. Catal.* **2002**, *207*, 37−45.
(45) Ilinitch, O. M.; Nosova, L. V.; Gorodetskii, V. V.; Ivanov, V. P.; Trukhan, S. N.; Gribov, E. N.; Bogdanov, S. V.; Cuperus, F. P. Catalytic reduction of nitrate and nitrite ions by hydrogen: investigation of the reaction mechanism over Pd and Pd−Cu catalysts. *J. Mol. Catal. A: Chem.* **2000**, *158*, 237−249.
(46) Hörold, S.; Vorlop, K. D.; Tacke, T.; Sell, M. Development of catalysts for a selective nitrate and nitrite removal from drinking water. *Catal. Today* **1993**, *17*, 21−30.
(47) Warn≪, J.; Turunen, I.; Salmi, T.; Maunula, T. Kinetics of nitrate reduction in monolith reactor. *Chem. Eng. Sci.* **1994**, *49*, 5763−5773.
(48) Pintar, A.; Batista, J.; Levec, J.; Kajiuchi, T. Kinetics of the catalytic liquid-phase hydrogenation of aqueous nitrate solutions. *Appl. Catal., B* **1996**, *11*, 81−98.
(49) Prüsse, U.; Hähnlein, M.; Daum, J.; Vorlop, K.-D. Improving the catalytic nitrate reduction. *Catal. Today* **2000**, *55*, 79−90.
(50) Daum, J.; Vorlop, K.-D. Kinetic Investigation of the Catalytic Nitrate Reduction: Construction of the Test Reactor System. *Chem. Eng. Technol.* **1999**, *22*, 199−202.
(51) Daub, K.; Emig, G.; Chollier, M. J.; Callant, M.; Dittmeyer, R. Studies on the use of catalytic membranes for reduction of nitrate in drinking water. *Chem. Eng. Sci.* **1999**, *54*, 1577−1582.
(52) Wen, J.; Xie, J.; Chen, X.; Li, X. A review on g-C_3N_4-based photocatalysts. *Appl. Surf. Sci.* **2017**, *391*, 72−123.
(53) Hankin, A.; Bedoya-Lora, F. E.; Alexander, J. C.; Regoutz, A.; Kelsall, G. H. Flat band potential determination: avoiding the pitfalls. *J. Mater. Chem. A* **2019**, *7*, 26162−26176.
(54) Hérissan, A.; Meichtry, J. M.; Remita, H.; Colbeau-Justin, C.; Litter, M. I. Reduction of nitrate by heterogeneous photocatalysis over pure and radiolytically modified TiO_2 samples in the presence of formic acid. *Catal. Today* **2017**, *281*, 101−108.
(55) Xu, P.; Agarwal, S.; Lefferts, L. Mechanism of nitrite hydrogenation over Pd/γ-Al_2O_3 according a rigorous kinetic study. *J. Catal.* **2020**, *383*, 124−134.
(56) Clark, C. A.; Reddy, C. P.; Xu, H.; Heck, K. N.; Luo, G.; Senftle, T. P.; Wong, M. S. Mechanistic Insights into pH-Controlled Nitrite Reduction to Ammonia and Hydrazine over Rhodium. *ACS Catal.* **2020**, *10*, 494−509.
(57) Jung, S.; Bae, S.; Lee, W. Development of Pd−Cu/Hematite Catalyst for Selective Nitrate Reduction. *Environ. Sci. Technol.* **2014**, *48*, 9651−9658.
(58) Jung, J.; Bae, S.; Lee, W. Nitrate reduction by maghemite supported Cu-Pd bimetallic catalyst. *Appl. Catal., B* **2012**, *127*, 148−158.

https://doi.org/10.1021/acsomega.1c05523
ACS Omega 2021, 6, 34850−34856